NANO LETTERS

2001
Vol. 1, No. 10
521−525

Mn-Substituted Inorganic–Organic Hybrid Materials Based on ZnSe: Nanostructures That May Lead to Magnetic Semiconductors with a Strong Quantum Confinement Effect

Harry R. Heulings IV, Xiaoying Huang, and Jing Li*

Department of Chemistry, Rutgers University, Camden, New Jersey 08102

Tan Yuen and C. L. Lin

Department of Physics, Temple University, Philadelphia, Pennsylvania 19122

Received May 22, 2001; *Revised Manuscript Received August 2, 2001*

ABSTRACT

Nanomaterials that make use of both electron charge and spin are highly desirable and extremely attractive in the development of new multifunctional devices for optoelectronics and information storage technology. In this study, we demonstrate that the hybrid nanostructures $Zn_{1-x}Mn_xSe(L)_{0.5}$ (L = ethylenediamine, 1,3-propanediamine) can be assembled with the substitution of Zn for Mn in the $ZnSe(L)_{0.5}$ systems. The latter are composed of perfectly ordered ZnSe semiconductor nanolayers interconnected via organic molecules coordinately bonded to act as "linkers" or "spacers". These hybrid nanostructures possess magnetically active periodic crystalline structures, which exhibit large blue shifts in their optical absorption edges (∼1.0–1.2 eV). Such shifts are a direct result of a very strong quantum confinement effect (QCE).

Recent advances in magnetoelectronics have opened new avenues to integrate functional materials that utilize both electron charge and spin.[1] Thus, the introduction of magnetic elements into nonmagnetic semiconductors allows for the generation of magnetic semiconductors. Such a development may lead to important applications in both optoelectronic and information storage technology.[2] Current studies have shown that ferromagnetism may be induced as a result of doping magnetic Mn onto nonmagnetic III−V and II−VI semiconductors.[3]

At the same time, an exciting and promising area of materials research that deals with synthesis, characterization, and modification of organic−inorganic hybrid composite materials is rapidly emerging.[4] These materials are likely to combine the superior electronic, magnetic, and optical properties, rigidity, and thermal stability of inorganic frameworks with the structural diversity, flexibility, processability, and other preferred properties (e.g., lightweight) of organic molecules to further enhance and improve their functionality and performance.

We have recently developed a synthetic strategy in assembling a unique class of inorganic−organic hybrid nanostructures $MQ(L)_{0.5}$ (M = Zn, Cd; Q = Se, Te; L = ethylenediamine or en, 1,3-propanediamine or pda). Similar to semiconductor quantum wells (QWs), these structures are composed of II−VI nanolayers. However, the II−VI nanolayers here are perfectly ordered via bridging organic spacers (L), which lead to periodic 3D crystal lattices.[5,6] The insulating organic layers impose a strong quantum confinement on the semiconductor layers and, consequently, a significant modification to the bulk properties. For example, very large blue shifts (1.0−1.5 eV) have been observed in their optical absorption edges.[5,6] These values are comparable to those generated by chemically grown and very small sized (2−5 nm) colloidal quantum dots (QDs) such as CdSe and InP (∼1.0 eV).[7] Calculations based on density functional theory using local density approximation (LDA) have shown that these blue shifts are indeed due to the strong quantum confinement effect (QCE) of the II−VI semiconductor.[5,6] Density of states (DOS) analysis has revealed that these nanolayers contribute significantly to the observed band-edge absorption. While colloidal quantum dots are highly capable in the tuning of electronic and optical properties of semiconductors on a large scale, uniformity in the particle size and periodic arrangement of dots remains a great challenge. For these systems to be practically useful in optical devices requiring sharp lines and strong intensity, particle size and periodic arrangement must be addressed.[8] The hybrid II−VI composite materials are particularly attractive because of their structural uniformity and periodicity.

10.1021/nl015556e CCC: $20.00
Published on Web 08/21/2001

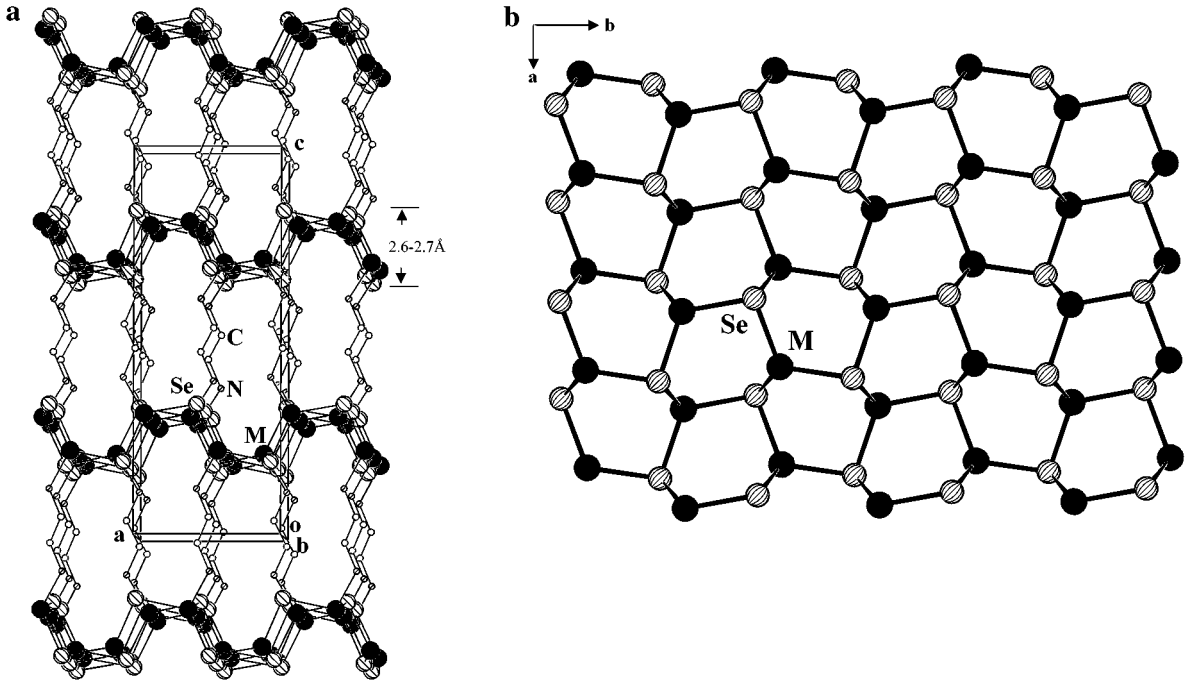

Figure 1. Crystal structure of $[MSe(en)_{0.5}]$, M = Mn (**1**), Zn (**3**). (a) View of $[MSe(en)_{0.5}]$ along the *b*-axis. Unit cell is outlined. The approximate thickness of the single atomic layer MSe is indicated. (b) The MSe 2D slab projected along the *c*-axis. The large solid circles are M, shaded circles Se, and small open and singly shaded circles C and N, respectively. All H atoms are omitted for clarity. Selected bond lengths (Å): (**1**), Mn−Se 2.5288(10), 2.5460(8) × 2 Å, Mn−N 2.179(4) Å; (**3**), Zn−Se 2.472(3), 2.446(4), 2.444(4) Å, Zn−N 2.157(15) Å.

One interesting question posed was whether magnetic elements can be introduced into these hybrid composite materials so that they not only can modify optical properties on a large scale but also can become magnetically active. In this letter, we describe our initial study on the Mn-substituted ZnSe-based hybrid composites and the optical and magnetic properties of these systems. Our approach involves three steps: (i) to obtain single-phased $ZnSe(L)_{0.5}$ and $MnSe(L)_{0.5}$ (L = en, pda) for the purpose of structural compatibility;[2] (ii) to substitute Zn by a magnetic element Mn in nonmagnetic $ZnSe(L)_{0.5}$ at various concentrations; and (iii) to investigate the optical and magnetic behavior of both unsubstituted and substituted nanostructures.

A solvothermal route was applied to the synthesis of $[MnSe(en)_{0.5}]$ (**1**), $[MnSe(pda)_{0.5}]$ (**2**), $[ZnSe(en)_{0.5}]$ (**3**), and $[ZnSe(pda)_{0.5}]$ (**4**).[6] Ethylenediamine and 1,3-propanediamine were used as *reactive solvents* (solvents that also act as reagents) in preparing these compounds. Both solvents entered the inorganic network via direct coordinated bonds. The crystal structures of **1** and **3** are isotypic.[9] It is a three-dimensional framework containing 2D [MSe] (M = Mn, Zn) slabs interconnected by bridging μ_2-en. A view of the structure along the *b*-axis is shown in Figure 1a. Alternating, three-coordinated M and Se atoms, in the slab, generate a puckered 6^3 honeycomb net (Figure 1b). A stable tetrahedral geometry of M is achieved by forming a fourth, coordinated bond to a bridging en molecule. As shown in Figure 2, the structure of **2** (and **4**) is closely related to **1** (and **3**).[10] The individual inorganic slabs in the two structures are nearly identical. However, the bridging μ_2-en in **1** (and **3**) is replaced by bridging μ_2-pda in **2** (and **4**). Moreover, the relative orientation of the slabs and the connectivity between the organic molecules and the inorganic slabs are somewhat different in the two structures (see Figure 1a and 2).

Substitution of Zn by Mn in $ZnSe(L)_{0.5}$ was successfully conducted at 140−160 °C.[11] Figure 3 shows powder X-ray diffraction (PXRD) patterns of the four representative systems, $Zn_{1-x}Mn_xSe(pda)_{0.5}$, with a Mn concentration of x = 0.0 (**4**), 0.25 (**5**), 0.5 (**6**), and 0.75 (**7**). No closely spaced, "doublet" peaks corresponding to multiple phases of $ZnSe(pda)_{0.5}$ and $MnSe(pda)_{0.5}$ were observed. The data clearly suggest that the samples were single-phased. The (200) peak shifts from 8.88° in the parent structure $ZnSe(pda)_{0.5}$ (a = 19.973 Å) to 8.80, 8.76, and 8.71° in 25%, 50%, and 75% Mn-substituted phases, respectively. The last is very close to the value of 8.68° in $MnSe(pda)_{0.5}$ (**2**) (a = 20.384 Å). The harmonic decrease in the (200) peak position (d spacing) is fully consistent with the increase in the Mn concentration and, consequently, the decrease in the unit cell dimensions.

The optical properties of **1**−**7** were assessed by diffuse reflectance experiments conducted at room temperature.[12] The optical spectra for **1**−**4** and **5**−**7** are plotted in Figure 4a,b, respectively. The spectra of α-MnSe (NaCl structure)[13] and ZnSe (Zinc Blende structure) measured under the same conditions, are also included in the figures as a comparison. The onset of the absorption edge is estimated to be 4.0 and 3.9 eV for **3** and **4**, respectively, corresponding to an enormous blue shift with respect to the band gap of the ZnSe bulk (2.5 eV). This large shift (1.4−1.5 eV) is attributed to the strong quantum confinement effect (QCE) due to the extremely small length scale of the thickness of the ZnSe single atomic monolayer in the hybrid structures (2.6−2.7

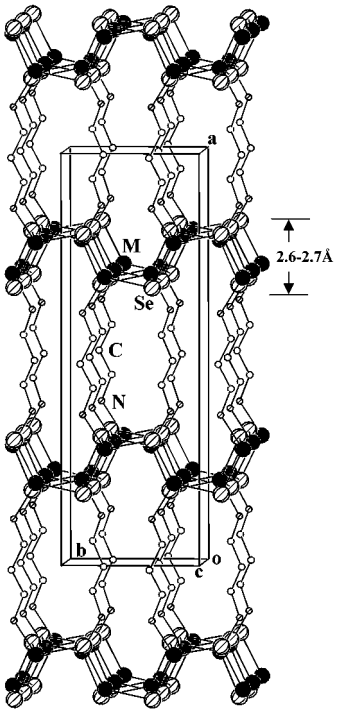

Figure 2. View of the crystal structure of $[MSe(pda)_{0.5}]$, M = Mn (**2**), Zn (**4**) along the *c*-axis with the unit cell outlined. The same labeling scheme as in Figure 1 is used here. All H atoms are omitted for clarity. The approximate thickness of the single atomic layer MSe is indicated in the figure. Selected bond lengths (Å): (**2**), Mn−Se 2.5237(13), 2.5465(16), 2.5475(13) Å, Mn−N 2.190(6) Å; (**4**), Zn−Se 2.435(4), 2.473(5), 2.471(4) Å, Zn−N 2.205(18) Å.

Å, Figures 1 and 2).[5,6] On the contrary, the estimated onset of the absorption edges for **1** and **2** is 1.8 and 1.7 eV, respectively. Clearly **1** and **2** give rise to changes in the same direction (increase in energy) with respect to bulk MnSe, but to a much lesser extent (0.1−0.2 eV), compared to the estimated band gap of 1.6 eV for MnSe.[14] This is due to the fact that the Mn 3d bands are highly localized, and therefore, the quantum confinement induced by coordinately bonded organic spacers[5] leads to a much smaller change in these bands.[15] All Mn-substituted hybrid systems exhibit a strong QCE even with high concentrations of Mn. This is demonstrated in Figure 4b. The onset of the absorption edges for 25%, 50%, and 75% Mn-substituted $Zn_{1-x}Mn_x(pda)_{0.5}$ are ∼3.7, 3.6, and 3.5 eV, respectively, giving rise to a blue shift of 1.0−1.2 eV with respect to 2.5 eV for the ZnSe bulk. Note that such shifts do not follow a linear dependence with respect to the composition. This is, most likely, due to the striking differences in the electronic structures of the two metals. As already pointed out, while Zn 3d bands are highly delocalized, the Mn 3d bands are very localized. Consequently, a linear increase in Mn concentration does not correspond to a linear shift in the absorption edges. The strong evidences provided by PXRD analysis showing that the samples are single-phased materials, are further supported by the results of the optical absorption experiments. Since the blue shifts (sharp band edge-like transitions), observed in the absorption spectra, are so dominating, they undoubt-

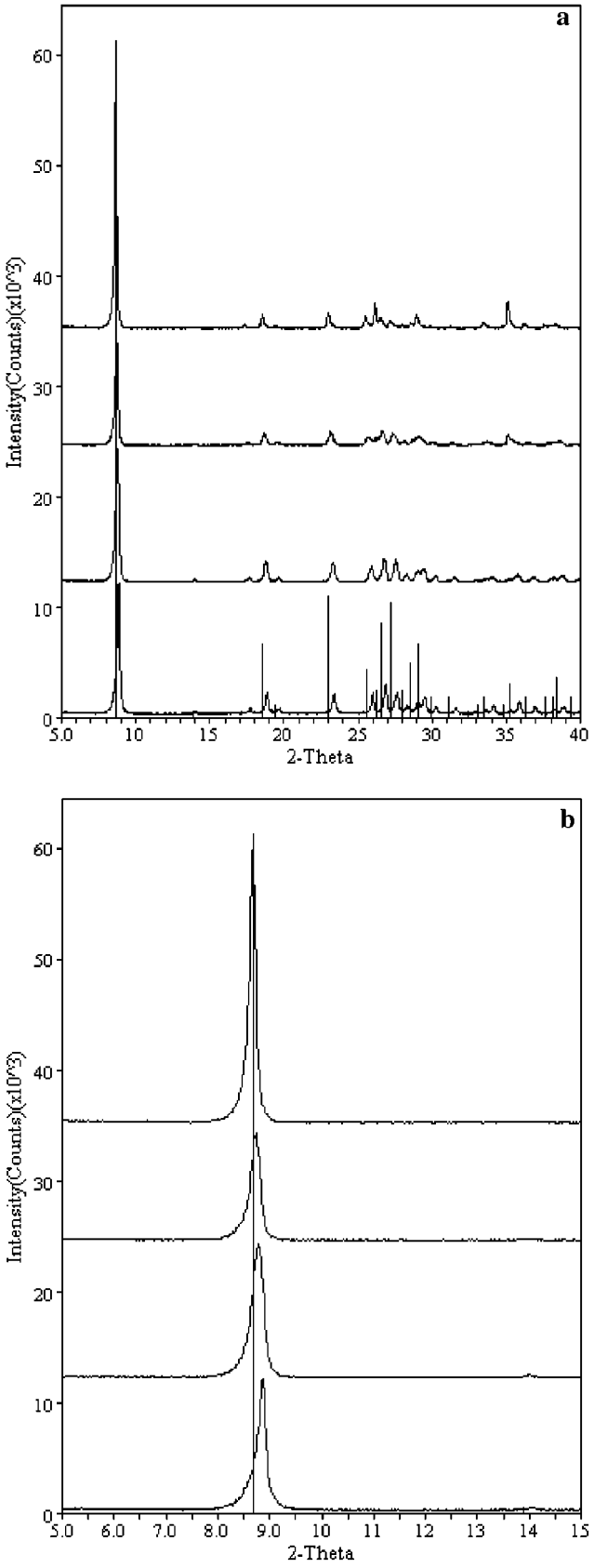

Figure 3. Powder X-ray diffraction patterns for **4**−**7**. (a) Spectra plotted in the 2θ range of 5−40°. The lines represented the simulated powder pattern of $MnSe(pda)_{0.5}$ from the single-crystal data. (b) Magnified PXRD patterns showing the (200) peaks. The (200) reflection of $MnSe(pda)_{0.5}$ is at $2\theta = 8.68°$.

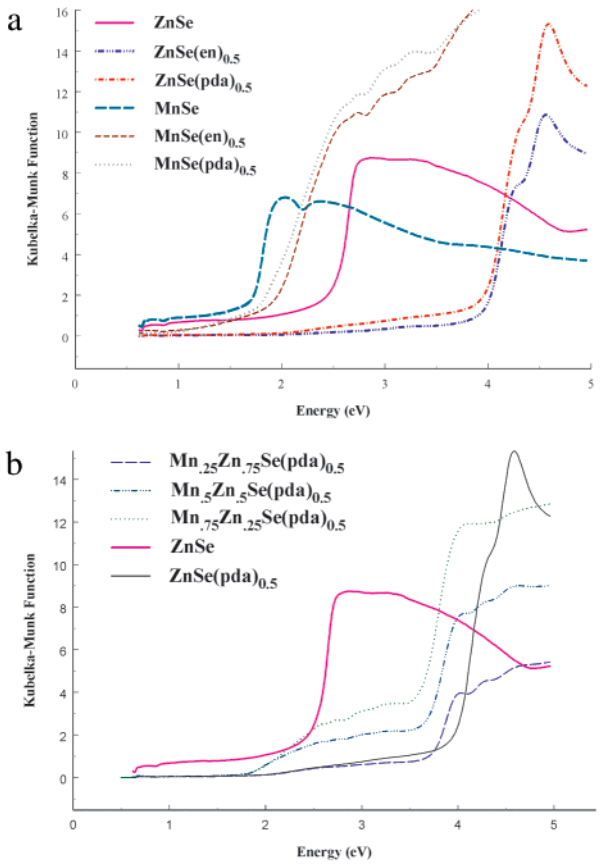

Figure 4. Optical absorption spectra for **1**−**4**. The measured spectra for bulk α-MnSe (NaCl structure) and ZnSe (zinc blende structure) are also plotted for comparison.

edly reflect the properties of the major phase (>97%) of the samples, i.e., $Zn_{1-x}Mn_xSe(L)_{0.5}$ ($0 < x \leq 1$) (Figure 4b). The small feature near the edge of ZnSe is possibly due to a minor impurity phase (most likely ZnSe), which constitutes less than 3% of the sample.

The results of field dependent magnetization $M(H)$ measurements[16] on **1**−**7** reveal paramagnetic behavior for all compounds, in that the $M(H)$ varies with H linearly. At 50 kG, M of **1** reaches a value of 478 emu/mol and M of **2** reaches a much higher value of 1190 emu/mol. There is no noticeable hesteresis observed in the $M(H)$ measurements for both compounds. The magnetic susceptibility is defined as $\chi(T) = M(T)/H$. Figure 5 shows χ as a function of T measured under an applied field of 1 kG for **1** and **2**. To see how much the $\chi(T)$ data deviate from the simple Curie law $\chi(T) = C/T$, the $1/\chi$ vs T plots are shown in the inset in Figure 5. The $\chi(T)$ data measured under other applied fields are essentially the same as $\chi(T)$ measured with a field of 1 kG. Also, there is almost no difference in the zero-field-cooled (ZFC) and field-cooled (FC) $\chi(T)$ data for all measurements. The $\chi(T)$ for both **1** and **2** indicate a paramagnetic state in all measured temperature ranges, which is consistent with the results of $M(H)$ measurements. However, it is noticed that in the $1/\chi$ vs T plots the $1/\chi$ curves intersect the T axis at negative temperature region, instead of intersecting the origin. Such behavior suggests a strong antiferromagnetic correlation between the Mn^{2+} ions in both compounds. In the temperature range 100−350 K, the $\chi(T)$

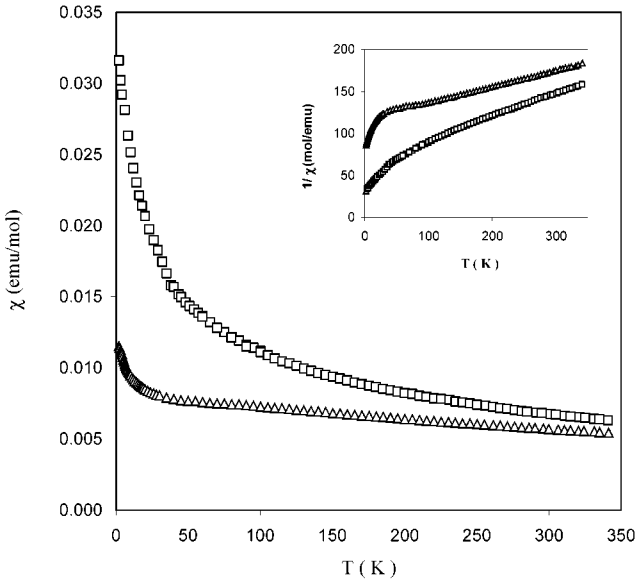

Figure 5. Magnetic susceptibility χ vs temperature T for **1** (Δ) and **2** (□). The insets are the $1/\chi$ vs T plots for the two compounds.

data were fit to Curie−Weiss law $\chi(T) = C/(T + \theta)$. From the fitting, we obtained the effective magnetic moment μ_{eff} values of 5.11 and 5.45 μ_B, for **1** and **2**, respectively. These μ_{eff} values are somewhat smaller than that obtained for MnSe (5.88 μ_B)[17] as well as the theoretical value of 5.92 μ_B for Mn^{2+}.[18] The fitted θ values for **1** and **2** are −465 and −235 K, suggesting strong antiferromagnetic interactions of the Mn^{2+} in these compounds.

The features observed in the magnetic measurements of **1** and **2** seem very similar, except that the anti-ferromagnetic coupling between Mn^{2+}, which is stronger in **1** than in **2** (possibly due to the fact that Mn−Mn distance is shorter in **1** than in **2**). The lack of a three-dimensional long range ordering in both **1** and **2** makes the magnetic properties of the two somewhat simple, compared to that of the starting material MnSe, an antiferromagnet with T_N around 249 K.[14] However, the results from the evaluation on the Mn:Zn concentration dependence study are rather interesting. Although the magnetization per unit formula of the "Mn/Zn alloying" compounds measured at 2 K and 55 kG increased as the ratio of Mn to Zn increased, the effective moment of M^{2+} decreased. In Figure 6, we show the χT vs T data for **5**, **6**, **7**, and **2**. As seen in the plot, there is a significant drop of χT from its room-temperature value to that of lower temperature, for all of the Mn/Zn compounds. This indicates the antiferromagnetic interaction between Mn^{2+}. A more important feature, in the data shown, is that the χT for smaller Mn concentrations is larger than that of higher Mn concentration in all temperature ranges. Such a variation of χT and related effective moments as a function of Mn concentration suggests that the introduction of Zn changes the electronic structure of MnSe significantly. The magnetic measurements on compounds with very low Mn concentrations ($x = 0.05$, 0.10, and 0.15) have also shown same variation of effective moment on x (not included in this report).

In summary, we have demonstrated the following: (a) Like their parent structures $ZnTe(L)_{1/2}$ and $ZnSe(L)_{1/2}$, Mn-

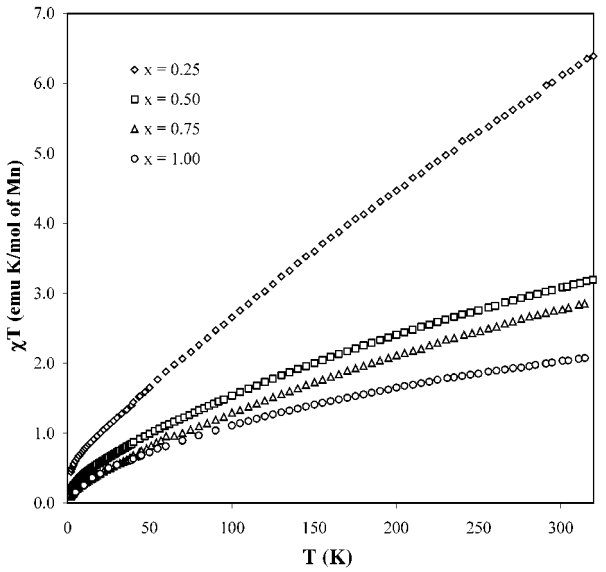

Figure 6. χT vs T plots for **5**, **6**, **7**, and **2**. Note that the unit in the y axis is (emu·K)/mol of Mn.

substituted hybrid nanocomposites $Zn_{1-x}Mn_xSe(L)_{1/2}$ (L = en, pda) can be synthesized via solvothermal reactions. The crystal structures of the substituted systems remain intact. (b) The substituted hybrid nanocomposites also exhibit a strong quantum confinement effect (QCE), reflected in the large blue shift in their optical absorption edges, as observed in the unsubstituted $ZnTe(L)_{1/2}$ and $ZnSe(L)_{1/2}$ systems. This strong quantum confinement effect is due to the large band offset between the inorganic and organic layers, which is supported by density functional calculations. The DOS analysis has revealed that highly confined II−VI single atomic monolayers (<1 nm) contribute extensively to the observed band-edge absorption.[5−6,19] The extent of changes in the optical properties depends largely on the amount of the magnetic substituents. (c) Substitution of Mn into nonmagnetic hybrid systems introduces large enhancement in the magnetic moments. It is found that the effective paramagnetic moment per Mn^{2+} decreases as the Mn concentration increases. The results from this preliminary study will guide our continuing efforts in the building of II−VI based hybrid nanocomposites with tailored magnetic and optical properties, which may contribute to the development in new multifunctional devices.

Acknowledgment. This work was generously supported by the National Science Foundation (DMR-0094872 and DMR-9633018).

References

(1) Prinz, G. A. *Science* **1998**, *282*, 1660.
(2) Ohno, H. *Science* **1998**, *281*, 951.
(3) Fiederling, R.; Keim, M.; Reuscher, G.; Ossau, W.; Schmidt, G.; Waag, A.; Molenkamp, L. W. *Nature* **1999**, *402*, 787. Ohno, Y.; Young, D. K.; Beschoten, B.; Matsukura, F.; Ohno, H.; Awschalom, D. D. *Nature* **1999**, *402*, 790. Dietl, T.; Ohno, H.; Matsukura, F.; Cibert, J.; Ferrand, D. *Science* **2000**, *287*, 1019.
(4) Kagan, C. R.; Mitzi, D. B.; Dimitrakopoulos, C. D. *Science* **1999**, *286*, 945. Batten, S. R.; Robson, R. *Angew. Chem., Int. Ed. Engl.* **1998**, *37*, 1460. Zaworotko, M. in *Electrical and Optical Polymer Systems*; Wise, D. I., Cooper, T. M., Gresser, J. D., Trantolo, D. J., Wnek, G. E., Eds.; Marcel Dekker: New York, 1998; p 871. Smith, J. V. *Chem. Rev.* **1988**, *88*, 149. Kressge, C. T.; Leonowicz, M. E.; Roth, W. J. Vartuni, J. C.; Beck, J. S. *Nature*, **1992**, *359*, 710. Mann, S.; Ozin, G. *Nature* **1996**, *382*, 313. Yang, P.; Zhao, D.; Margolese, D. I.; Chmelka, B. F.; Stucky, G. D. *Nature* **1998**, *396*, 152. Inagaki, S.; Guan, S.; Fukushima, Y.; Ohsuna, T.; Terasaki, O. *J. Am. Chem. Soc.* **1999**, *121*, 9611. Asefa, T.; MacLachlan, M. J.; Coombs, N.; Ozin, G. A. *Nature* **1999**, *402*, 867.
(5) Huang, X.-Y.; Li, J.; Fu, H.-X. *J. Am. Chem. Soc.* **2000**, *122*, 8789.
(6) Huang, X.-Y.; Heulings IV, H. R.; Le, V. L.; Li, J. *Chem. Mater.*, in press.
(7) Murray, C. B.; Norris, D. J.; Bawendi, M. G. *J. Am. Chem. Soc.* **1993**, *115*, 8706. Empedocles, S. A.; Norris, D. J.; Bawendi, M. G. *Phys. Rev. Lett.* **1996**, *77*, 3873.
(8) Murray, C. B.; Kagan, C. R.; Bawendi, M. G. *Science* **1995**, *270*, 1335. Nozik, A. J.; Micic, O. I. *MRS Bull.* **1998**, *23*, 24.
(9) Crystal Structure of **1**: $C_2H_8N_2Se_2Mn_2$, $M = 327.90$, 0.18 × 0.15 × 0.02 mm, orthorhombic, space group *Pbca*, $a = 6.711(1)$, $b = 6.614(1)$, $c = 17.720(4)$ Å, $V = 786.5(2)$ Å^3, $Z = 4$, $F(000) = 608$, $\rho_{calc.} = 2.769$ g cm^{-3}, μ(Mo Kα) = 12.372 mm^{-1}. $R = 0.0278$, $wR = 0.0655$. Crystal Structure of **3**: $C_2H_8N_2Se_2Zn_2$, $M = 348.76$, orthorhombic, space group *Pbca*, $a = 6.6298(9)$, $b = 6.4608(9)$, $c = 17.350(2)$ Å, $V = 743.17(17)$ Å^3, $Z = 4$, $F(000) = 648$, $\rho_{calcd} = 3.117$ g cm^{-3}, μ(Mo Kα) = 16.15 mm^{-1}. Rietveld refinement on powder X-ray diffraction data, $R_p = 0.0877$, $R_{wp} = 0.1345$.
(10) Crystal Structure of **2**: $C_3H_{10}N_2Se_2Mn_2$, $M = 341.93$, 0.20 × 0.10 × 0.02 mm, orthorhombic, space group $Cmc2_1$, $a = 20.384(4)$, $b = 6.719(1)$, $c = 6.565(1)$ Å, $V = 899.1(3)$ Å^3, $Z = 4$, $F(000) = 640$, $\rho_{calcd} = 2.526$ g cm^{-3}, μ(Mo Kα) = 10.829 mm^{-1}, $R = 0.0367$, $wR = 0.0886$. Crystal Structure of **4**: $C_3H_{10}N_2Se_2Zn_2$, $M = 362.79$, orthorhombic, space group $Cmc2_1$, $a = 19.9770(18)$, $b = 6.6286(6)$, $c = 6.4409(6)$ Å, $V = 852.89(14)$ Å^3, $Z = 4$, $F(000) = 680$, $\rho_{calcd} = 2.825$ g cm^{-3}, μ(Mo Kα) = 14.08 mm^{-1}. Rietveld refinement on powder X-ray diffraction data, $R_p = 0.112$, $R_{wp} = 0.161$.
(11) All reactions were carried out in sealed evacuated Pyrex tubes. All reaction products were cooled to room temperature and washed with 80% and 30% ethanol followed by drying in anhydrous ethyl ether. Compound **5** was synthesized solvothermally in a 1,3-propanediamine solution (pda, 0.4 mL) containing 0.0157 g of $MnCl_2$ (0.125 mmol), 0.0245 g of Zn (0.375 mmol), 0.0395 g of Se (0.5 mmol) in the mole ratio of 0.25:0.75:1. The sample was heated at 160 °C for 6 days. Light-tan powder was collected. Reaction of $MnCl_2$ (0.0315 g, 0.25 mmol), Zn (0.0163 g, 0.25 mmol), Se (0.0395 g, 0.5 mmol), and pda (0.4 mL) in a mole ratio of 0.5:0.5:1:10 at 160 °C for 8 days afforded tan powder of **6**. Orange-tan powder of **7** was obtained by reactions of $MnCl_2$ (0.0472 g, 0.375 mmol), Zn (0.0082, 0.125 mmol), Se (0.0395 g, 0.5 mmol), and pda (0.45 mL) in a mole ratio 0.75:0.25:1:11 at 140 °C for 8 days.
(12) Optical diffuse reflectance measurements of **1**−**7** were performed on a Shimadzu UV-3101PC double-beam, double-monochromator spectrophotometer. Data were collected and converted using the Kubelka−Munk function. See: Wendlandt, W. WM.; Hecht, H. G. *Reflectance Spectroscopy*, Interscience: A Division of John Wiley & Sons: New York, 1966. Li, J.; Chen, Z.; Wang, X.-X.; Proserpio, D. M. *J. Alloys Compounds* **1997**, *262*−*263*, 28.
(13) The most stable structure form of MnSe is the NaCl structure. See: Baroni, A. *Z. Kristallogr., Kristallgeom., Kristallphysik, Kristallchem.* **1938**, *99*, 336.
(14) Note that the measured value for MnSe (1.6 eV) is somewhat smaller than the previously reported E_g. Decker, D. L.; Wild, R. L. *Phys. Rev. B* **1971**, *4*, 3425.
(15) Sato, H.; Mihara, T.; Furuta, A.; Tamura, M.; Mimura, K.; Happo, N.; Taniguchi, M. *Phys. Rev. B* **1997**, *56*, 7222.
(16) Magnetic measurements on polycrystalline samples of **1**−**7** were performed using a Quantum Design SQUID magnetometer. These measurements include the field dependent magnetization $M(H)$ and magnetic susceptibility $\chi(T)$, defined as $M(T)/H$. Temperature in the $\chi(T)$ measurements was varied from 2 to 350 K. For each compound, we performed both zero-field-cooled (ZFC) and field-cooled (FC) measurements of $\chi(T)$ under several magnetic fields. $M(H)$ was measured at 2 K for all samples. In the $M(H)$ measurements, the applied magnetic field was increased from 0 to 50 kG and then decreased back to 0 G.
(17) Ito, T.; Ito, K.; Oka, M. *Jpn. J. Appl. Phys.* **1978**, *17*, 371.
(18) Kettel, C. *Introduction to Solid State Physics*; John Wiley & Sons: New York, 1986.
(19) Fu, H.-X.; et al. Unpublished results.

NL015556E